Dehydrogenation of Formic Acid Catalyzed by an Osmium-Polyhydride: Relevance of Acid Assistance in the CO_2 Formation Stage

Miguel A. Esteruelas, Ana M. López, Enrique Oñate, and Esther Raga*

Departamento de Química Inorgánica, Instituto de Síntesis Química y Catálisis Homogénea (ISQCH), Centro de Innovación en Química Avanzada (ORFEO-CINQA), Universidad de Zaragoza-CSIC, 50009 Zaragoza, Spain.

ABSTRACT: Complex $OsH_4\{\kappa^1\text{-}P,\eta^2\text{-}GeH\text{-}[^iPr_2PCH(Me)CH_2GeEt_2H]\}(P^iPr_3)$ (**1**) breaks down formic acid into H_2 and CO_2. The decomposition is catalytic with complex **1** being the main metallic species detected spectroscopically during the process. The kinetic analysis of the catalysis reveals that the decomposition rate is first order in the catalyst and independent of the concentration of formic acid, with the calculated activation parameters being: $\Delta H^{\ddagger}$ = 23 ± 2 kcal mol^{-1}, $\Delta S^{\ddagger}$ = -1 ± 5 cal mol^{-1} K^{-1}, and $^{298}\Delta G^{\ddagger}$ = 23 ± 3 kcal mol^{-1}. Complex **1** also shows stoichiometric reactivity with benzoic and acetic acids. The reactions lead to $OsH_2\{\kappa^2\text{-}O,O\text{-}[O_2CR]\}\{\kappa^2\text{-}P,Ge\text{-}[^iPr_2PCH(Me)CH_2GeEt_2]\}(P^iPr_3)$ (R = Ph (**9**), Me (**10**)). On the basis of these findings and DFT calculations, the following mechanism for the decomposition is proposed:

complex **1** releases one molecule of H_2 to produce an osmium(IV)-trihydride unsaturated intermediate, which promotes heterolytic activation of the O−H bond of formic acid. The metal fragment of the resulting osmium(IV)-(κ^1-*O*-formate) saturated derivative slides along the formate group, following the O–C–H pathway. The displacement is assisted externally by a molecule of formic acid and generates an osmium(IV)-(κ^1-*H*-formate) species, which releases CO_2 to regenerate **1** and close a cycle. The dissociation of H_2 from the latter is the rate-determining step of catalysis.

INTRODUCTION

The number of homogeneous catalysts based on transition metal polyhydride complexes is small compared to the number of homogeneous transition metal catalysts from classical families. However, the scarce members of this particular family are particularly promising[1] for several reasons. The MH_n unit that forms the polyhydride can give rise to three different types of H-donating ligands: Kubas-type dihydrogen, elongated dihydrogen, and hydride.[2] They can coexist in the same species, while each of them interacts with the metal center in a different way.[3] Furthermore, H-donating ligands can exchange their positions in solution and transform into each other.[4] Because each type of ligand has different chemical behavior,[5] polyhydride complexes show superior chemical versatility to other families of transition metal complexes, revealed in part by their ability to activate a spectacular range of σ-bonds.[6] This capacity, the non-innocent character of the hydride ligand,[7] and the ease of the metal center to transfer hydrides to unsaturated organic molecules make polyhydride complexes one of the most versatile families of catalysts.[1]

Polyhydride catalysts are emerging as exceptionally useful tools for implementing hydrogen technology. Molecular hydrogen has an energy content per mass approximately three times greater

than that of petroleum-derived fuels. However, its energy content per volume is low at standard temperature and pressure, making it difficult to transport and handle. In this context, the concept of chemical hydrogen storage makes sense, because several chemical compounds have a reasonable hydrogen content that can be easily released on demand, in the presence of a catalyst.[8] Because of their high hydrogen content, amine-boranes, particularly ammonia-borane, are among the most promising chemical candidates for hydrogen storage. These materials are dehydrogenated by some polyhydride complexes in an efficient and kinetically controlled manner,[9] but their disadvantage is that they are difficult to recycle.[10] A feasible alternative is some organic liquids or low-melting solids, including alkanes, amines, alcohols, or formic acid.[11] These chemical hydrogen deposits are also catalytically dehydrogenated in the presence of some polyhydride complexes[12] and, in contrast to amine-boranes, can reversibly undergo metal-promoted hydrogenation.[1] Furthermore, as a result of their easy handling, they are compatible with current transportation and refueling infrastructures.

Formic acid is considered one of the most serious options for the future. Although it only contains a 4.4% by weight, it provides a volumetric content of the vector equivalent to 1.77 kWh L^{-1}, in its decomposition into H_2 and CO_2 (eq 1 in Chart 1), as a consequence of its high density (1.22 g mL^{-1}). Such value exceeds that of current industry standard storage tanks, around 1.4 kWh L^{-1}. Furthermore, it is produced on a large scale and is easy to handle under ambient conditions, due to its low flammability and toxicity.[13] The recyclability of this carboxylic acid is also constantly being improved, in which polyhydrides of iron,[14] ruthenium,[15] and iridium[16] play a prominent role through the hydrogenation of CO_2. On the contrary, the catalytic performance of polyhydride complexes in the decomposition of formic acid into H_2 and CO_2 is very poor. Catalysts based on representative elements[17] and 3d metals[18] have been used; nevertheless, the state of the

art still focuses on the 4d and 5d elements,[19] mainly ruthenium,[20] rhodium,[21] and iridium;[22] with some recent palladium-based examples.[23] However, none of them belong to the polyhydride family. Known polyhydride catalysts are reduced to osmium derivatives **I**[24] and **II**[25] (Chart 1), consistent with the richness of osmium-polyhydride chemistry.[6,26]

Chart 1. Known Polyhydride Catalysts for Formic Acid Dehydrogenation

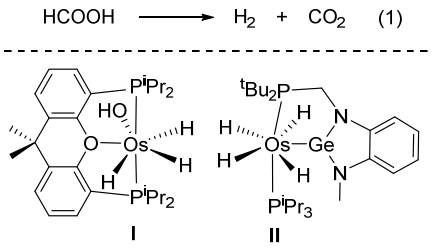

Complex **II** is a bifunctional catalyst formed by a basic metal and an σ-donor and π-acceptor Z-type acidic ligand;[27] pioneer in inverting the electron density flow direction, as the Os(IV)–Ge(II) bond enhances the basicity of the osmium basic center and the acidity of the acidic germylene ligand. As a consequence, it works differently than traditional bifunctional catalysts (Scheme 1). The rapid step involving H_2 formation occurs exclusively in the basic osmium coordination sphere, while both the metal center and the σ-donor Lewis acid cooperatively promote the rate-determining release of CO_2.[25] Thus, the latter can be seen as an intramolecular acid-assisted process, as the formate group rotates around the Ge–O bond to bring its hydrogen atom closer to the osmium center.

Scheme 1. Catalytic Cycle for the Formic Acid Dehydrogenation Promoted by Complex II

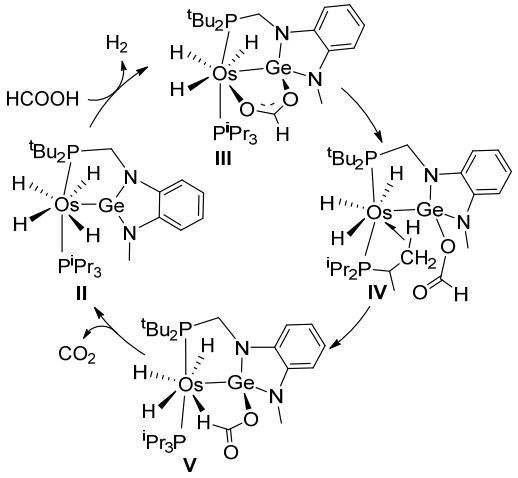

We have recently observed that one of the phosphine ligands of the hexahydride $OsH_6(P^iPr_3)_2$ undergoes germylation with Et_3GeH, through metathesis between Ge−C(sp^3) and H−C(sp^3) bonds. The hexahydride complex reacts with the germanium-hydride to initially produce a rare pentahydride-osmium(VI)-germyl intermediate, $OsH_5(GeEt_3)(P^iPr_3)_2$, which evolves to the σ-germane derivative $OsH_4\{\kappa^1\text{-}P,\eta^2\text{-}GeH\text{-}[^iPr_2PCH(Me)CH_2GeEt_2H]\}(P^iPr_3)$ (**1**). The transformation involves the displacement of one of the substituents of the germyl ligand by a methyl group of an isopropyl substituent of the phosphine involved (Scheme 2).[28] Unlike the germanium atom of germylenephosphine of **II**, the germanium atom of this other bidentate (η^2-GeH)-phosphine ligand has the electrons necessary to achieve electronic saturation. In search for the differences between both systems and trying to delve deeper into the role of acid-assistance during the CO_2 release process, we decided to investigate the catalytic performance of the σ-complex **1** in the dehydrogenation of formic acid.

Scheme 2. Formation of Complex 1

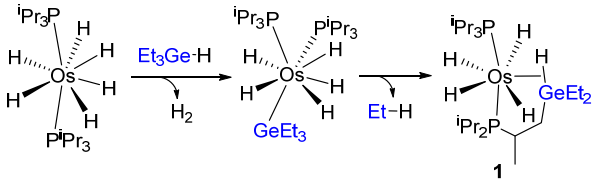

This paper presents a new polyhydride catalyst for the dehydrogenation of formic acid and its working method, supported by the kinetic analysis of the catalysis, DFT calculations, and stoichiometric reactions. Furthermore, it demonstrates the relevance of acid assistance; when intramolecular aid is not possible, it is produced intermolecularly using the substrate itself as an external source.

RESULTS AND DISCUSSION

Formic Acid Dehydrogenation: Kinetic Study. Complex **1** catalyzes the decomposition of formic acid to quantitatively produce H_2 and CO_2 according to eq 1 (Chart 1). During the dehydrogenation, the only metallic species detected by $^{31}P\{^1H\}$ NMR spectroscopy is the catalyst itself, which is recovered unchanged at the end of the decomposition. The catalytic reactions were performed in toluene, in a closed reactor under constant volume conditions, between 333 and 373 K, with catalyst and acid concentrations in the ranges 0.53−2.60 x 10^{-2} M and 0.26−0.79 M, respectively. To obtain information on the catalyst performance and regarding the decomposition mechanism, the kinetics of the catalysis was investigated under pseudo-first-order conditions. The partial pressure of the generated hydrogen (P_{H_2}; atm) was determined according to eq 2, where P_T and P_{CO_2} are respectively the total pressure and the partial pressure of CO_2.

$$P_{H_2} = P_T - P_{CO_2} \qquad (2)$$

The initial rates of H_2 formation were obtained from the gas evolution experiments using eq 3, where V is the reactor volume (L), R is the ideal gas constant, T is the temperature of reaction (K) and V_{sol} is the volume of the solution (L). Table 1 summarizes the values obtained under each particular experimental condition of temperature and concentration of catalyst and formic acid, whereas Figure 1a exemplifies the course of the reactions carried out at different concentrations of catalyst, at 363 K, and an initial concentration of acid ($[HCO_2H]_0$) of 0.53 M.

$$\frac{d[H_2]}{dt} = \left(\frac{dP_{H_2}}{dt}\right)\frac{V}{RTV_{sol}} \qquad (3)$$

Table 1. Kinetic Data for the Dehydrogenation of Formic Acid Catalyzed by 1

T (K)	[**1**] (10^2 M)	$[HCO_2H]_0$ (M)	$d[H_2]/dt$ (10^2 M min^{-1})	k (min^{-1})
363	0.53	0.53	0.20	0.38
363	0.91	0.53	0.38	0.42
363	1.06	0.53	0.44	0.42
363	1.60	0.53	0.73	0.46
363	2.60	0.53	1.14	0.44
363	1.60	0.26	0.72	0.45
363	1.60	0.40	0.72	0.45
363	1.60	0.66	0.73	0.46
363	1.60	0.79	0.71	0.45
333	1.60	0.53	0.03	0.02
343	1.60	0.53	0.11	0.07
353	1.60	0.53	0.31	0.20
373	1.60	0.53	1.66	1.04

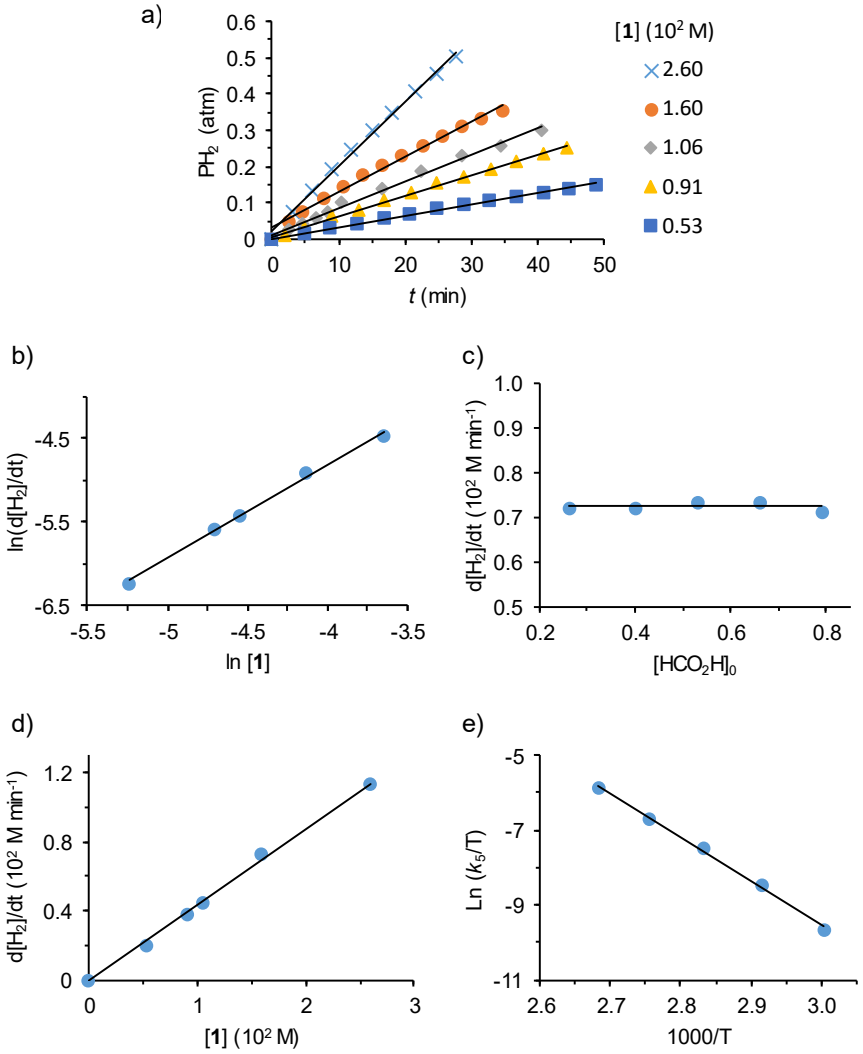

Figure 1. a) Plot of P_{H_2} vs time at different concentrations of **1** in toluene (T = 363 K, $[HCO_2H]_0$ = 0.53 M). b) Plot of ln(d$[H_2]$/dt) *vs* ln [**1**] (T = 363 K, $[HCO_2H]_0$ = 0.53 M). c) Plot of d$[H_2]$/dt *vs* $[HCO_2H]_0$ (T = 363 K, [**1**] = 1.60×10^{-2} M). d) Plot of d$[H_2]$/dt *vs* [**1**] (T = 363 K, $[HCO_2H]_0$ = 0.53 M). e) Eyring plot for the catalytic dehydrogenation of formic acid in toluene ([**1**] = 1.60×10^{-2} M, $[HCO_2H]_0$ = 0.53 M).

The rate law for the formation of H_2 from the decomposition of formic acid catalyzed by **1** can be obtained by the general mathematical expression given in eq 4:

$$\frac{\mathrm{d}[\mathrm{H_2}]}{\mathrm{d}t} = k[\mathbf{1}]^a[\mathrm{HCO_2H}]_0{}^b \qquad (4)$$

Both reaction orders were determined at 363 K. The plot of ln(d[H_2]/dt) *vs* ln[**1**] produces a straight line with a slope of 1.1±0.1 (Figure 1b), for reactions performed with $[HCO_2H]_0$ = 0.53 M. This supports a first order in the catalyst concentration; a = 1 in eq 4. Unlike catalyst concentration, the rate of H_2 formation is independent of $[HCO_2H]_0$, for a fixed [**1**] = 1.6 × 10^{-2} M (Figure 1c), which reveals that b = 0 in eq 4. Thus, the rate law is:

$$\frac{\mathrm{d}[\mathrm{H_2}]}{\mathrm{d}t} = k[\mathbf{1}] \qquad (5)$$

Figure 1d shows the plot of d[H_2]/dt vs [**1**], at 363 K, which yields a value for k at this temperature of 0.44 ± 0.04 min^{-1}. The Eyring analysis in the temperature range studied (Figure 1e) allows the activation parameters to be calculated: $\Delta H^{\ddagger}$ = 23 ± 2 kcal mol^{-1} and $\Delta S^{\ddagger}$ = -1 ± 5 cal mol^{-1} K^{-1}, which leads to a $\Delta G^{\ddagger}$ value of 23 ± 3 kcal mol^{-1} at 298 K.

The efficiency of a catalyst in a given reaction has traditionally been evaluated on the basis of the turnover frequency (TOF) value provided by this catalyst. However, it is now clearly established that only the standard turnover frequency (TOF^0) value allows a rigorous evaluation, to be compared, of the catalytic performance of a particular species in a reaction.[29] Unfortunately, TOF^0 values are rarely reported. Thus, the experimental value of $\Delta G^{\ddagger}$ at 298 K of the reaction in the presence of the catalyst becomes a more reasonable measure of the efficiency of said catalyst. The $\Delta G^{\ddagger}$ values at 298 K reported for the dehydrogenation of formic acid catalyzed by homogeneous transition metal systems is in the range of 17–26 kcal mol^{-1}.[1,22c,24,25,30] The value of $\Delta G^{\ddagger}$ at 298 K obtained for **1** lies in the central part of this range, which indicates that complex **1** is a catalyst of medium efficiency, similar to that of complex **II**.

The metal-catalyzed dehydrogenation of formic acid has two stages: formation of H_2 and formation of CO_2. The rate law given in eq 5 and the finding of **1** as the major metallic species during decomposition suggest that the rate-determining step in this case is the formation of H_2. Thus, the mechanism of catalysis can be summarized as follows: complex **1** slowly loses a H_2 molecule to produce an unsaturated intermediate, which rapidly extracts hydrogen atoms from the acid to regenerate **1** releasing CO_2.

DFT Calculations about the Mechanism. To gain insight into the intimate details of the mechanism, we performed DFT (SMD-(toluene)-wB97XD//SDD/cc-pVDZ) calculations on both stages of the decomposition. The ΔG values were calculated at 298.15 K and 1 atm. Figure 2 shows the calculated reaction profile, whereas Scheme 3 compiles the optimized intermediates contextualizing their roles in the catalysis.

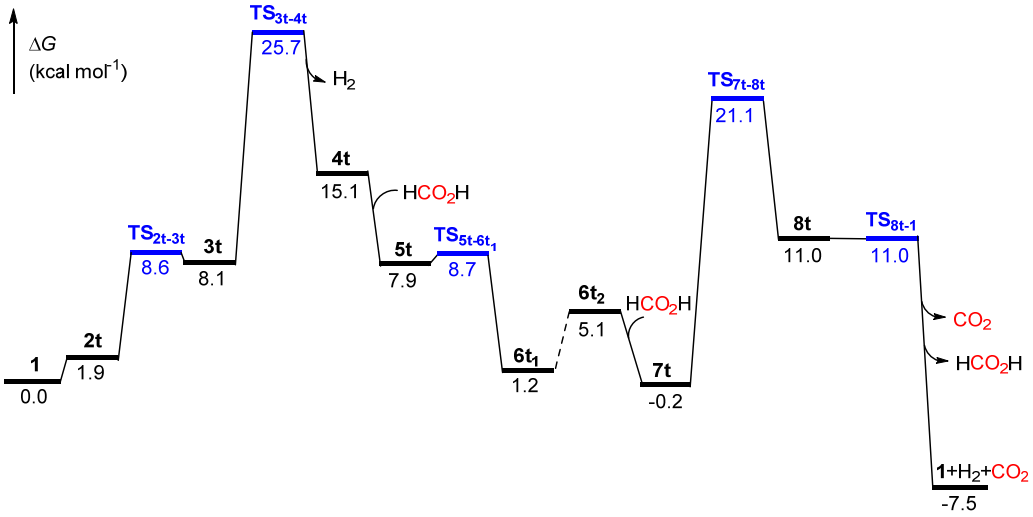

Figure 2. DFT energy profile for the formic acid dehydrogenation catalyzed by **1**.

Scheme 3. Catalytic Cycle for the Formic Acid Dehydrogenation Catalyzed by 1

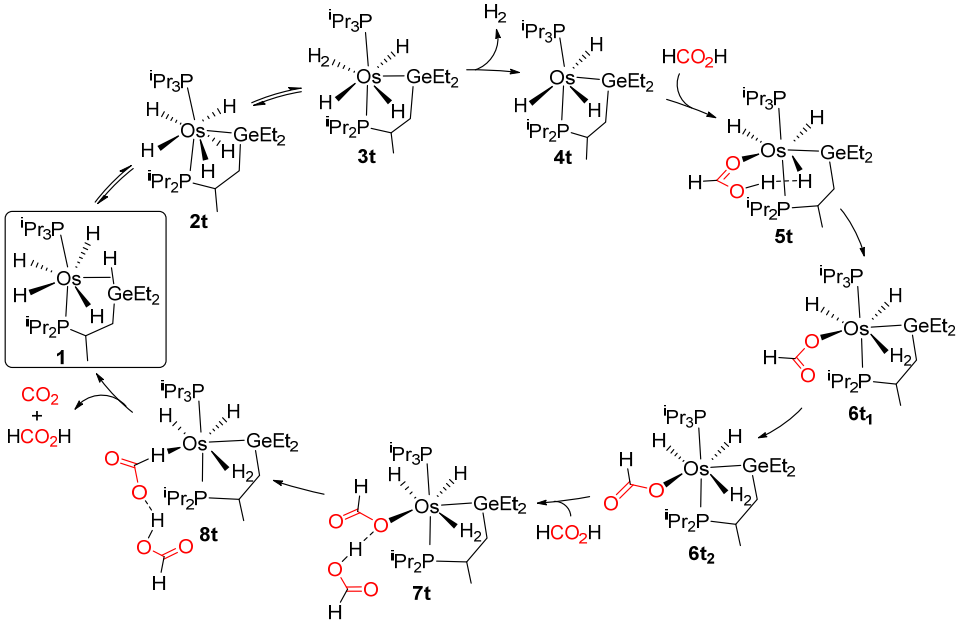

The DFT calculations reveal that complex **1** is in equilibrium with the derivatives osmium(VI)-pentahydride **2t** and trihydride-osmium(IV)-(Kubas-type dihydrogen) **3t**. These species are respectively 1.9 kcal mol^{-1} and 8.1 kcal mol^{-1} less stable than **1**. The first results from the homolytic cleavage of the Ge–H coordinated bond. The oxidative addition gives rise to the dodecahedral structure typical of the eight-coordinate osmium-polyhydride complexes.[31] The dodecahedron is defined by two intersecting orthogonal trapezoidal planes; one of them contains the phosphorus atoms and two hydride ligands, while the other is formed by the remaining three hydrides and the germanium atom. The transformation of the hydride ligands located in the *P,H,H,P*-plane into a Kubas-type dihydrogen (H–H = 0.936 Å) and the simultaneous reduction of the metal center provides **3t**. The release of the coordinated hydrogen molecule leads to the unsaturated osmium(IV)-trihydride **4t**. Dissociation occurs through the transition state $\mathbf{TS_{3t\text{-}4t}}$, which is 25.7 kcal mol^{-1} above **1**. This value is similar to that obtained for $\Delta G^{\ddagger}$ at 298 K, from the Eyring analysis shown in the Figure 1e. Furthermore, it consistently represents the highest barrier of the profile.

Intermediate **4t** promotes heterolytic activation of the O–H bond of the acid, using one of the hydride ligands as an internal base. The activation is directed by the other oxygen atom. Thus, initially the saturated species **5t** is formed, which exhibits an electrostatic interaction between the acidic hydrogen atom of the coordinated formic acid and a neighboring hydride. The interaction is strongly supported by the separation between the involved atoms of 1.347 Å, which is much shorter than the sum of the Van der Waals radii (rvdw(H) = 1.20 Å),[32] and the Mulliken and NBO charges of the hydride (-0.165 and -0.231) and the hydrogen atom of formic acid (+0.280 and +0.485). It can be qualified as a dihydrogen bond.[33] The transfer of the proton from the acid to the hydride generates a Kubas-type dihydrogen ligand (H–H = 0.916 Å). The resulting intermediate **6t$_1$** has a κ^1-*O*-formate group on its osmium coordination sphere. The hydrogen atom of this group is located away from the metal center, in the opposite direction to it. Therefore, the formate group must pivot on the oxygen atom attached to the metal to bring the hydrogen atom closer to the latter. The process gives rise to **6t$_2$**, which is a rotamer of **6t$_1$**, 3.9 kcal mol^{-1} less stable. The intermediate **6t$_2$** is a saturated species and therefore a β-hydrogen elimination reaction is not possible to remove the hydrogen atom from the formate group. Then, the formate-coordinating fragment is forced to slide toward the hydrogen atom, following the O–C–H path. The sliding allows the release of CO_2 and the regeneration of **1**, but the barrier to be overcome, 27.1 kcal mol^{-1} with respect to **1**, is higher than the activation energy corresponding to the elimination of H_2 from **1** and that of the catalytic reaction. Consequently, this pathway is not experimentally consistent, although the barrier could be in principle energetically accessible.

It has been observed that the rate of formic acid dehydrogenation catalyzed by some transition metal complexes increases dramatically by adding Lewis acids to the catalytic solution.[18c] Given the participation of the acidic germylene center in the CO_2 formation stage of the process catalyzed

by **II** (Scheme 1),[25] we reasoned that the acidic OH hydrogen atom of formic acid could also perform some positive function in this particular case. In fact, we find that an electrostatic interaction between this atom of a second formic acid molecule and the osmium-bonded oxygen atom of **6t₂** stabilizes the system up to a value of 0.2 kcal mol^{-1} below **1**. The formation of the hydrogen bond in 7**t** adduct facilitates the sliding of the metal fragment through the O–C–H path, reducing the barrier for CO_2 release to 21.1 kcal mol^{-1}.[34] The second formic acid molecule does not directly participate in the slippage; the binding of its OH hydrogen atom to the osmium-attached oxygen atom seems to reduce the coordination power of such atom, which opens the door for the movement of the metal. The new barrier is 4.6 kcal mol^{-1} lower than the DFT activation energy calculated for the hydrogen dissociation from **1**, which corresponds to the rate-determining step of catalysis. Thus, this formic acid-assisted pathway for CO_2 release is experimentally consistent. It occurs in two steps through the adduct intermediate **8t**. This species is the direct result from the slippage and, unlike **7t**, coordinates the formate group through the hydrogen atom. Intermediate **8t** releases CO_2 and the second molecule of formic acid, regenerating **1**, in a barrier-free process that also liberates 7.5 kcal mol^{-1} with respect to **1**.

Stoichiometric Reactions with Benzoic and Acetic Acids. In the search for evidence on the existence and nature of the intermediates that live between the steps involving the H_2 dissociation and the CO_2 release, we also analyzed the reactivity of **1** towards carboxylic acids unable of undergoing the reaction shown in eq 1. The treatment of solutions of **1**, in toluene, with 1.1 equiv of benzoic and acetic acids, at 60 ºC, for 24 h produces the release of 2.0 equiv of H_2 and the formation of the osmium(IV)-dihydride derivatives $OsH_2\{\kappa^2\text{-}O,O\text{-}[O_2CR]\}\{\kappa^2\text{-}P,Ge\text{-}[^iPr_2PCH(Me)CH_2GeEt_2]\}(P^iPr_3)$ (R = Ph (**9**), Me (**10**); Scheme 4). These products are consistent with the formation of the **6t₁** intermediate and therefore their generation can be rationalized

through the **4t** intermediate. The heterolytic activation of the O–H bond of acids promoted by **4t** would initially lead to derivatives analogous to **6t$_1$**; **^{R}6t$_1$**. Subsequent displacement of the Kubas-type dihydrogen ligand by the free oxygen atom of the respective κ^1-*O*-carboxylate group should yield the isolated compounds.

Scheme 4. **Preparation of complexes 9 and 10**

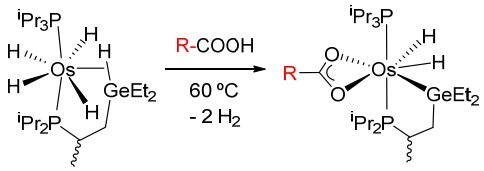

1 R = Ph (**9**), Me (**10**)

Complexes **9** and **10** were isolated as yellow solids in 68 % and 59 % yield, respectively. The coordination geometry proposed for these species in Scheme 4 was corroborated by X-ray diffraction analysis on a single crystal of the acetate derivative **10**. The structure has two chemically equivalent but crystallographically independent molecules in the asymmetric unit, which correspond to the enantiomeric pair of one of the diastereoisomers resulting from the chirality of both the C(1) atom of the κ^2-*P,Ge*-ligand and the metal center. Figure 3 offers a view of one of these enantiomers. The coordination polyhedron around the osmium atom can ideally be described as a pentagonal bipyramid with the phosphorus atoms of the phosphine ligands in apical positions (P(1)−Os(1)−P(2) = 168.30(2)º and 171.44(2)º). The hydride ligands are located at the base between the chelate carboxylate group and the germanium atom.

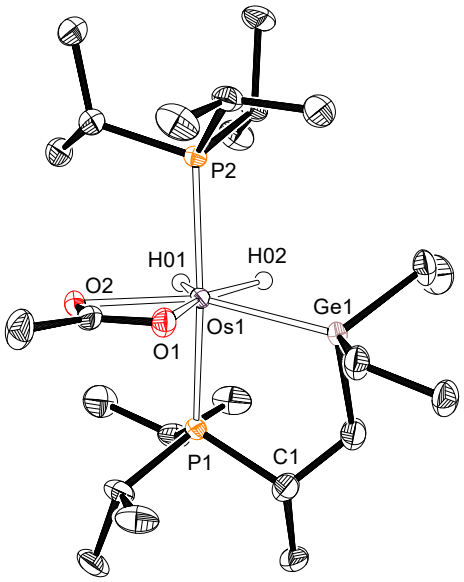

Figure 3. X-ray structure of one of the two independent molecules of **10** in the asymmetric unit with 50% probability ellipsoids. Hydrogen atoms (except hydrides) are omitted for clarity. Selected bond lengths (Å) and angles (deg) for the X-ray structure: Os(1)−P(1) = 2.3677(5), 2.3480(5), Os(1)−P(2) = 2.3818(5), 2.3709(5), Os(1)−Ge(1) = 2.4122(2), 2.4888(3), Os(1)−O(1) = 2.2910(15), 2.2251(15), Os(1)−O(2) = 2.1701(14), 2.2528(15); P(1)−Os(1)−P(2) = 168.305(19), 171.439(18), Ge(1)−Os(1)−P(1) = 82.040(14), 82.204(15), Ge−Os(1)−P(2) = 104.508(14), 102.402(15).

The diastereisomers of **9** and **10** participate in a rapid epimerization equilibrium, in solution, at room temperature. Thus, the $^{31}P\{^{1}H\}$ NMR spectra of both compounds, in toluene-d_8, between 243 K and 298 K show an AB spin system centered around 43 ppm, which clearly becomes two AB spin systems at 193 K and 183 K, respectively (Figures S8 and S13). The ^{1}H NMR spectra support such an equilibrium and reveal that the hydride ligands are furthermore involved in a thermally activated position exchange process. At room temperature, they contain a broad double doublet due to inequivalent hydride ligands ($T_{1(min)}$ = 102−133 ms), at about -16.8 ppm, which converts to four signals at temperatures below 193 K (Figures S9 and S14). The epimerization

process probably occurs through five-coordinate unsaturated hydride-osmium(II)-carboxylate intermediates (**A** in Scheme 5), which result from a Ge−H reductive elimination. The metal center of said intermediates oxidatively re-adds the Ge−H bond on the O-Os-H side opposite to that of the reductive elimination.

Scheme 5. **Epimerization of Complexes 9 and 10**

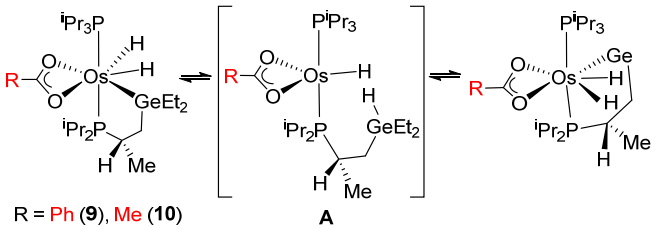

CONCLUDING REMARKS

This study has revealed that complex **1** catalyzes the decomposition of formic acid into H_2 and CO_2. The kinetic study of catalysis, DFT calculations, and stoichiometric reactions involving **1** and benzoic and acetic acids allow us to make a solid proposal on the mechanism of the dehydrogenation. Complex **1** releases one molecule of H_2 to produce an osmium(IV)-trihydride unsaturated intermediate, which promotes a heterolytic activation of the O–H bond of formic acid. The metal fragment of the resulting saturated osmium(IV)-(κ^1-*O*-formate) derivative slides along the formate group, following the O−C−H pathway. The displacement is assisted externally by a formic acid molecule and generates an osmium(IV)-(κ^1-*H*-formate) species, which releases CO_2 to regenerate **1** and close a cycle. The dissociation of H_2 from the latter is the rate-determining step of catalysis.

Three legs support mechanistic research in catalysis: kinetic analysis, DFT calculations, and stoichiometric reactions. It should be noted that the comparison of the mechanism deduced on this

solid basis for the dehydrogenation of formic acid catalyzed by two related systems, previously **II** (Scheme 1)[25] and now **1** (Scheme 3), shows as a similarity the need to assist the CO_2 formation stage with an acid center. This underlines the importance of acid assistance, which occurs even in the absence of added Lewis acids. In such a case, it can be provided internally by some ligand of the catalyst such as germylene of **II** or externally by a second molecule of formic acid itself, when the catalyst does not have any acid center as in **1**.

Experimental Section

General Information. The reactions were carried out under argon using dried solvents and Schlenk-tube techniques. Instrumental methods, X-ray information, and DFT computational details are provided in the Supporting Information. Complex **1** was prepared according to the published method.[28] Chemical shifts are expressed in ppm and coupling constants are given in Hertz.

Formic Acid Dehydrogenation. The progress of the catalytic reactions was monitored using a reactor fitted out with a pressured transducer (Man on the Moon series X103 kit; https://manonthemoontech.com/x104-gas-evolution). The total volume of the reactor was 18.8 mL. Under an argon atmosphere, a solution of **1** in 1 mL of toluene was added into the reactor, which was closed and placed in an oil bath at the desired temperature. Once the pressure was stabilized, the reactor was tared. After that, the formic acid was added with a syringe through a septum cap. This moment was taken as the initial time of the catalysis. The reaction was followed by registering the total pressure as a function of time. Pressures were calculated according to the ideal gas law. Since we deal with the evolution of two moles of gas (H_2 and CO_2) per mol of HCOOH, the total pressure is divided by two and applied to calculate the rate of H_2 formation.

Preparation of $OsH_2\{\kappa^2$-*O,O*-$[O_2CPh]\}\{\kappa^2$-*P,Ge*-$[^iPr_2PCH(Me)CH_2GeEt_2]\}(P^iPr_3)$ (9). A mixture of **1** (62.5 mg, 0.097 mmol) and benzoic acid (13.0 mg, 0.11 mmol) in toluene (4 mL) was stirred in a screw cap Schlenk-tube at 60 ºC for 24 h. After cooling the resulting suspension, the solvent was evaporated until ca. 2 mL. A yellow solid was obtained by decantation, which was washed with MeOH at -78 ºC (3 x 2 mL), and dried in vacuo. Yield: 50 mg (68%). Anal. Calcd. for $C_{29}H_{58}GeO_2OsP_2$: C, 45.62; H, 7.66. Found: C, 45.58; H, 7.76. HRMS (electrospray, *m*/*z*): calcd. for $C_{29}H_{58}GeO_2OsP_2$ $[M]^+$: 766.2733; found 766.2700. IR (cm^{-1}): ν(Os-H) 2154 (w), ν(OCO) 1523 (s), 1498 (s). ^{1}H NMR (300.13 MHz, C_6D_6, 298K): δ 8.17−8.10 (m, 2H, Ph), 7.14−7.04 (m, 3H, Ph), 2.30−2.14 (4H, 3 PCH P^iPr_3 + PCH P^iPr_2), 2.10-1.96 (m, 1H, PCH P^iPr_2), 1.83−1.66 (m, 1H, PCH P^iPr_2), 1.49−1.17 (38H, 10H $GeEt_2$ + 18H PCC*H*$_3$ P^iPr_3 + 9H PCC*H*$_3$ P^iPr_2 + 1H PCHC*H*$_2$Ge), 1.08 (dd, $^3J_{H,P}$ = 12.8, $^3J_{H,H}$ = 6.9, 3H, PCC*H*$_3$ P^iPr_2), 1.00 (dd, $^3J_{H,P}$ = 11.1, $^3J_{H,H}$ = 7.0, 3H, PCC*H*$_3$ P^iPr_2), 0.88 (ddd, $^2J_{H,H}$ = $^3J_{H,H}$ = 12.8, $^3J_{H,P}$ = 4.7, 1H, PCC*H*$_2$Ge), -16.70 (br dd, $^2J_{H,P}$ = 11.90, 2H, Os-H). $^{31}P\{^1H\}$ NMR (121.50 MHz, C_6D_6, 298 K): δ 43.5 (AB spin system, Δν = 3289 Hz, $J_{A\text{-}B}$ = 266.5 Hz). $^{13}C\{^1H\}$-apt NMR (75 MHz, C_6D_6, 298 K): δ 177.2 (s, *C*OOPh), 135.8 (s, C_q Ph), 131.7, 128.3, 128.2 (all s, Ph), 32.3 (d, $J_{C,P}$ = 26.3, PCH P^iPr_2), 27.5 (dd, $J_{C,P}$ = 22.5, 3.7, PCH*C*H$_2$Ge), 27.2 (dd, $J_{C,P}$ = 20.3, 1.5, PCH P^iPr_3), 24.5 (dd, $J_{C,P}$ = 21.0, 2.5, PCH P^iPr_2), 23.9 (dd, $J_{C,P}$ = 21.8, 1.0, PCH P^iPr_2), 20.1 (PC*C*H$_3$ P^iPr_3 + 1 PC*C*H$_3$ P^iPr_2), 19.6 (d, $^2J_{C,P}$ = 2.3, PC*C*H$_3$ P^iPr_2), 19.3 (d, $^2J_{C,P}$ = 2.3, PC*C*H$_3$ P^iPr_2), 18.6 (d, $^2J_{C,P}$ = 3, PC*C*H$_3$ P^iPr_2), 18.5 (d, $^2J_{C,P}$ = 3, 2 PC*C*H$_3$ P^iPr_2), 11.5 (s, Ge*C*H$_2$CH$_3$), 11.0, 10.9 (both s, GeCH$_2$*C*H$_3$), 10.2 (s, Ge*C*H$_2$CH$_3$). ^{1}H NMR (400 MHz, toluene-d_8, 243 K, high-field region): δ -16.40 (br, 1H, OsH_2), -16.80 (br, 1H, OsH_2). $T_{1(min)}$ (ms, OsH_2, 400 MHz, toluene-d_8, 243 K): 126 ± 12 (-16.40 ppm), 133 ± 13 (-16.80 ppm).

Preparation of $OsH_2\{\kappa^2$-*O,O*-$[O_2CMe]\}\{\kappa^2$-*P,Ge*-$[^iPr_2PCH(Me)CH_2GeEt_2]\}(P^iPr_3)$ (10). A mixture of **1** (125 mg, 0.194 mmol) and acetic acid (12.2 μL, 0.21 mmol) in toluene (4 mL) was stirred in a screw cap Schlenk-tube at 60 ºC for 24 h. The solvent was evaporated under vacuum and addition of MeOH at -78 ºC to the resulting yellow oil caused the precipitation of a yellow solid, which was washed with MeOH at -78 ºC (3 x 2 mL), and dried in vacuo. Yellow single crystals suitable for XRD analysis were grown by slow diffusion of pentane into a solution of **10** in toluene at -30 ºC. Yield: 80 mg (59%). Anal. Calcd. for $C_{24}H_{56}GeO_2OsP_2$: C, 41.09; H, 8.05. Found: C, 40.89; H, 7.80. HRMS (electrospray, m/z): calcd. for $C_{24}H_{56}GeO_2OsP_2$ $[M]^+$: 704.2579; found 704.2557. IR (cm^{-1}): ν(Os-H) 2187, 2148 (w), ν(OCO) 1541, 1456 (s). ^{1}H NMR (300.13 MHz, C_6D_6, 298 K): δ 2.32−2.16 (4H, 3 PCH P^iPr_3 + PCH P^iPr_2), 2.12−2.00 (m, 1H, PCH P^iPr_2), 1.79−1.67 (m, 1H, PCH P^iPr_2), 1.65 (s, 3H, COOMe), 1.51−1.14 (38H, 10H $GeEt_2$ + 18H PCC*H*$_3$ P^iPr_3 + 9H PCC*H*$_3$ P^iPr_2 + 1H PCHC*H*$_2$Ge), 1.11 (dd, $^3J_{H,P}$ = 12.5, $^3J_{H,H}$ = 7.0, 3H, PCC*H*$_3$ P^iPr_2), 1.07 (dd, $^3J_{H,P}$ = 10.7, $^3J_{H,H}$ = 7.0, 3H, PCC*H*$_3$ P^iPr_2), 0.80 (ddd, $^2J_{H,H}$ = $^3J_{H,H}$ = 12.8, $^3J_{H,P}$ = 4.6, 1H, PCC*H*$_2$Ge), -16.90 (br dd, $^2J_{H,P}$ = 11.4, 2H, Os-H). ^{31}P{^{1}H} NMR (121.50 MHz, C_6D_6, 298 K): δ 43.4 (AB spin system, Δν = 3263 Hz, $J_{A,B}$ = 269.7 Hz). ^{13}C{^{1}H}-apt NMR (75 MHz, C_6D_6, 298 K): δ 182.4 (s, *C*OOMe), 32.0 (d, $^1J_{C,P}$ = 27.3, PCH P^iPr_2), 27.5 (dd, $J_{C,P}$ = 22.4, 3.6, PCH*C*H$_2$Ge), 27.4 (dd, $J_{C,P}$ = 20.4, 1.6, PCH P^iPr_3), 26.2 (s, COO*Me*), 24.7, 23.8 (both d, $^1J_{C,P}$ = 21.4, PCH P^iPr_2), 20.2 (s, PC*C*H$_3$ P^iPr_2), 20.0, 20.0 (both s, PC*C*H$_3$ P^iPr_3), 19.5 (d, $^2J_{C,P}$ = 2.8, PC*C*H$_3$ P^iPr_2), 19.1 (d, $^2J_{C,P}$ = 1.5, PC*C*H$_3$ P^iPr_2), 18.6 (m, 2 PC*C*H$_3$ P^iPr_2), 11.3 (s, Ge*C*H$_2$CH$_3$), 10.9, 10.8 (both s, GeCH$_2$*C*H$_3$), 9.8 (s, Ge*C*H$_2$CH$_3$). ^{1}H NMR (400 MHz, toluene-d_8, 253 K, high-field region): δ -16.60 (br, 1H, OsH_2), -17.10 (br, 1H, OsH_2). $T_{1(min)}$ (ms, OsH_2, 400 MHz, toluene-d_8): 106 ± 10 (233 K, -16.60 ppm), 102 ± 10 (243 K, -17.10 ppm).

ASSOCIATED CONTENT

Supporting Information

The Supporting Information is available free of charge on the ACS publications web site.

General information for the experimental section, crystallographic data, computational details, catalytic reaction profiles, and NMR spectra (PDF)

Cartesian coordinates of the optimized structures (XYZ)

Accession codes

CCDC 2330447 contains the crystallographic data for this paper. These data can be obtained free of charge *via* www.ccdc.cam.ac.uk/data_request/cif, or by e-mailing data_request@ccdc.cam.ac.uk, or by contacting The Cambridge Crystallographic Data Centre, 12 Union Road, Cambridge CB2 1EZ, UK; fax: +44 1223 336033.

AUTHOR INFORMATION

Corresponding Author

* E-mail: maester@unizar.es.

Notes

The authors declare no competing financial interest.

ACKNOWLEDGMENT

Financial support from MICIN/AEI/10.13039/501100011033 (PID2020-115286GB-I00 and RED2022-134287-T), Gobierno de Aragón (E06_23R), FEDER, and the European Social Fund is acknowledged. E. R. thanks the MICINN for her FPI contract (PRE2018-085398, “ESF investing

in your future"). The CESGA Supercomputing Center and BIFI Institute are also acknowledged for the use of their computational resources.

REFERENCES

(1) Babón, J. C.; Esteruelas, M. A.; López, A. M. Homogeneous catalysis with polyhydride complexes. *Chem. Soc. Rev.* **2022**, *51*, 9717–9758.

(2) (a) Kubas, G. J. Metal Dihydrogen σ-Bond Complexes: Structure, Theory and Reactivity. Kluwer, New York, 2001. (b) Kubas, G. J. Fundamentals of H_2 Binding and Reactivity on Transition Metals Underlying Hydrogenase Function and H_2 Production and Storage. *Chem. Rev*. **2007**, *107*, 4152−4205. (c) Crabtree, R. H. Dihydrogen Complexation. *Chem. Rev.* **2016**, *116*, 8750−8769.

(3) Maseras, F.; Lledós, A.; Clot, E.; Eisenstein, O. Transition Metal Polyhydrides: From Qualitative Ideas to Reliable Computational Studies. *Chem. Rev*. **2000**, *100*, 601−636.

(4) Morris, R. H. Dihydrogen, dihydride and in between: NMR and structural properties of iron group complexes. *Coord. Chem. Rev.* **2008**, *252*, 2381–2394.

(5) Eguillor, B.; Esteruelas, M. A.; Lezáun, V.; Oliván, M.; Oñate, E. Elongated Dihydrogen versus Compressed Dihydride in Osmium Complexes. *Chem. Eur. J.* **2017**, *23*, 1526−1530.

(6) Esteruelas, M. A.; López, A. M.; Oliván, M. Polyhydrides of Platinum Group Metals: Nonclassical Interactions and σ-Bond Activation Reactions. *Chem. Rev.* **2016**, *116*, 8770−8847.

(7) (a) Esteruelas, M. A.; Fernández, I.; García-Yebra, C.; Martín, J.; Oñate, E. Elongated σ-Borane versus σ-Borane in Pincer-POP-Osmium Complexes. *Organometallics* **2017**, *36*,

2298−2307. (b) Babón, J. C.; Esteruelas, M. A.; Fernández, I.; López, A. M.; Oñate, E. Evidence for a Bis(Elongated σ)-Dihydrideborate Coordinated to Osmium. *Inorg. Chem.* **2018**, *57*, 4482−4491. (c) Esteruelas, M. A.; Martínez, A.; Oliván, M.; Oñate, E. Direct C−H Borylation of Arenes Catalyzed by Saturated Hydride-Boryl-Iridium-POP Complexes: Kinetic Analysis of the Elemental Steps. *Chem. Eur. J.* **2020**, *26*, 12632−12644.

(8) (a) El-Shafie, M.; Kambara, S.; Hayakawa, Y. Hydrogen Production Technologies Overview. J. *Power. Energy. Eng.* **2019**, *7*, 107−154. (b) Le, P.-A.; Trung, V. D.; Nguyen, P. L.; Phung, T. V. B.; Natsuki, J.; Natsuki, T. The current status of hydrogen energy: an overview. *RSC Adv*. **2023**, *13*, 28262–28287.

(9) (a) Esteruelas, M. A.; López, A. M.; Mora, M.; Oñate, E. Ammonia-Borane Dehydrogenation Promoted by an Osmium Dihydride Complex: Kinetics and Mechanism. *ACS. Catal.* **2015**, *5*, 187−191. (b) Rossin, A.; Peruzzini, M. Ammonia-Borane and Amine-Borane Dehydrogenation Mediated by Complex Metal Hydrides. *Chem. Rev.* **2016**, *116*, 8848−8872. (c) Adams, G. M.; Colebatch, A. L.; Skornia, J. T.; McKay, A. I.; Johnson, H. C.; Lloyd-Jones, G. C.; Macgregor, S. A. Beattie, N. A.; Weller, A. S. Dehydropolymerization of $H_3B{\cdot}NMeH_2$ To Form Polyaminoboranes Using [Rh(Xantphos-alkyl)] Catalysts. *J. Am. Chem. Soc.* **2018**, *140*, 1481−1495. (d) Colebatch, A. L.; Weller, A. S. Amine-Borane Dehydropolymerization: Challenges and Opportunities. *Chem. Eur. J.* **2019**, *25*, 1379−1390. (e) Brodie, C. N.; Boyd, T. M.; Sotorríos, L.; Ryan, D. E.; Magee, E.; Huband, S.; Town, J. S.; Lloyd-Jones, G. C.; Haddleton, D. M.; Macgregor, S. A.; Weller, A. S. Controlled Synthesis of Well-Defined Polyaminoboranes on Scale Using a Robust and Efficient Catalyst. *J. Am. Chem. Soc.* **2021**, *143*, 21010−21023.

(10) Whittell, G. R.; Manners, I. Advances with Ammonia-Borane: Improved Recycling and Use as a Precursor to Atomically Thin BN Films. *Angew. Chem. Int. Ed.* **2011**, *50*, 10288−10289.

(11) Modisha, P. M.; Ouma, C. N. M.; Garidzirai, R.; Wasserscheid, P.; Bessarabov, D. The Prospect of Hydrogen Storage Using Liquid Organic Hydrogen Carriers. *Energy Fuels* **2019**, *33*, 2778−2796.

(12) (a) Bertoli, M.; Choualeb, A.; Gusev, D. G.; Lough, A. J.; Major, Q.; Moore, B. PNP pincer osmium polyhydride for catalytic dehydrogenation of primary alcohols. *Dalton Trans.* **2011**, *40*, 8941−8949. (b) Schleker, P. P. M.; Honeker, R.; Klankermayer, J.; Leitner, W. Catalytic Dehydrogenative Amide and Ester Formation with Rhenium-Triphos Complexes. *ChemCatChem* **2013**, *5*, 1762−1764. (c) Esteruelas, M. A.; Lezáun, V.; Martínez, A.; Oliván, M.; Oñate, E. Osmium Hydride Acetylacetonate Complexes and Their Application in Acceptorless Dehydrogenative Coupling of Alcohols and Amines and for the Dehydrogenation of Cyclic Amines. *Organometallics* **2017**, *36*, 2996−3004. (d) Buil, M. L.; Esteruelas, M. A.; Gay, M. P.; Gómez-Gallego, M.; Nicasio, A. I.; Oñate, E.; Santiago, A.; Sierra, M. A. Osmium Catalyst for Acceptorless and Base-Free Dehydrogenation of Alcohols and Amines: Unusual Coordination Modes of a BPI Anion. *Organometallics* **2018**, *37*, 603−617. (e) Buil, M. L.; Esteruelas, M. A.; Izquierdo, S.; Nicasio, A. I.; Oñate, E. N−H and C−H Bond Activations of an Isoindoline Promoted by Iridium- and Osmium-Polyhydride Complexes: A Noninnocent Bridge Ligand for Acceptorless and Base-Free Dehydrogenation of Secondary Alcohols. *Organometallics* **2020**, *39*, 2719−2731. (f) Cancela, L.; Esteruelas, M. A.; Oliván, M.; Oñate, E. Azolium Control of the Osmium-Promoted Aromatic C−H Bond Activation in 1,3-Disubstituted Substrates. *Organometallics* **2021**, *40*, 3979−3991. (g) Gordon, B. M.; Lease, N.; Emge, T. J.; Hasanayn, F.; Goldman, A. Reactivity of Iridium Complexes of a Triphosphorus-Pincer Ligand Based on a Secondary Phosphine.

Catalytic Alkane Dehydrogenation and the Origin of Extremely High Activity. *J. Am. Chem. Soc.* **2022**, *144*, 4133−4146.

(13) Kawanami, H.; Himeda, Y.; Laurency, G. Formic Acid as a Hydrogen Carrier for Fuel Cells Toward a Sustainable Energy System. *Adv. Inorg. Chem.* **2017**, *70*, 395−427.

(14) (a) Federsel, C.; Boddien, A.; Jackstell, R.; Jennerjahn, R.; Dyson, P. J.; Scopelliti, R.; Laurenczy, G.; Beller, M. A Well-Defined Iron Catalyst for the Reduction of Bicarbonates and Carbon Dioxide to Formates, Alkyl Formates, and Formamides. *Angew. Chem. Int. Ed.* **2010**, *49*, 9777−9780. (b) Ziebart, C.; Federsel, C.; Anbarasan, P.; Jackstell, R.; Baumann, W.; Spannenberg, A.; Beller, M. Well-Defined Iron Catalyst for Improved Hydrogenation of Carbon Dioxide and Bicarbonate. *J. Am. Chem. Soc.* **2012**, *134*, 20701−20704.

(15) Estes, D. P.; Leutzsch, M.; Schubert, L.; Bordet, A.; Leitner, W. Effect of Ligand Electronics on the Reversible Catalytic Hydrogenation of CO_2 to Formic Acid Using Ruthenium Polyhydride Complexes: A Thermodynamic and Kinetic Study. *ACS Catal.* **2020**, *10*, 2990−2998.

(16) (a) Tanaka, R.; Yamashita, M.; Nozaki, K. Catalytic Hydrogenation of Carbon Dioxide Using Ir(III)−Pincer Complexes. *J. Am. Chem. Soc.* **2009**, *131*, 14168−14169. (b) Tanaka, R.; Yamashita, M.; Chung, L. W.; Morokuma, K.; Nozaki, K. Mechanistic Studies on the Reversible Hydrogenation of Carbon Dioxide Catalyzed by an Ir-PNP Complex. *Organometallics* **2011**, *30*, 6742−6750.

(17) (a) Myers, T. W.; Berben, L. A. Aluminium-ligand cooperation promotes selective dehydrogenation of formic acid to H_2 and CO_2. *Chem. Sci.* **2014**, *5*, 2771–2777. (b) Chauvier, C.;

Tlili, A.; Das Neves Gomes, C.; Thuéry, P.; Cantat, T. Metal-free dehydrogenation of formic acid to H_2 and CO_2 using boron-based catalysts. *Chem. Sci.* **2015**, *6*, 2938–2942.

(18) (a) Boddien, A.; Loges, B.; Gärtner, F.; Torborg, C.; Fumino, K.; Junge, H.; Ludwig, R.; Beller, M. Iron-Catalyzed Hydrogen Production from Formic Acid. *J. Am. Chem. Soc.* **2010**, *132*, 8924−8934. (b) Boddien, A.; Mellmann, D.; Gärtner, F.; Jackstell, R.; Junge, H.; Dyson, P. J.; Laurenczy, G.; Ludwig, R.; Beller, M. Efficient Dehydrogenation of Formic Acid Using an Iron Catalyst. *Science* **2011**, *333*, 1733−1736. (c) Bielinski, E. A.; Lagaditis, P. O.; Zhang, Y.; Mercado, B. Q.; Würtele, C; Bernskoetter, W. H.; Hazari, N.; Schneider, S. Lewis Acid-Assisted Formic Acid Dehydrogenation Using a Pincer-Supported Iron Catalyst. *J. Am. Chem. Soc.* **2014**, *136*, 10234−10237. (d) Anderson, N. H.; Boncella, J.; Tondreau, A. M. Manganese-Mediated Formic Acid Dehydrogenation. *Chem. Eur. J*. **2019**, *25*, 10557–10560. (e) Léval, A.; Junge, H.; Beller, M. Manganese(I) κ^2-*NN* complex-catalyzed formic acid dehydrogenation. *Catal. Sci. Technol.* **2020**, *10*, 3931−3937. (f) Curley, J. B.; Bernskoetter, W. H.; Hazari, N. Additive-Free Formic Acid Dehydrogenation Using a Pincer-Supported Iron Catalyst. *ChemCatChem* **2020**, *12*, 1934−1938. (g) Léval, A.; Agapova, A.; Steinlechner, C.; Alberico, E.; Junge, H.; Beller, M. Hydrogen production from formic acid catalyzed by a phosphine free manganese complex: investigation and mechanistic insights. *Green Chem.* **2020***, 22,* 913−920. (h) Lentz, N.; Aloisi, A.; Thuéry, P.; Nicolas, E.; Cantat, T. Additive-Free Formic Acid Dehydrogenation Catalyzed by a Cobalt Complex. *Organometallics* **2021**, *40*, 565−569.

(19) (a) Guo, J.; Yin, C. K.; Zhong, D. L.; Wang, Y. L.; Qi, T.; Liu, G. H.; Shen, L. T.; Zhou, Q. S.; Peng, Z. H.; Yao, H.; Li, X. B. Formic Acid as a Potential On-Board Hydrogen Storage Method: Development of Homogeneous Noble Metal Catalysts for Dehydrogenation Reactions. *ChemSusChem* **2021**, *14*, 2655−2681. (b) Younas, M.; Rezakazemi, M.; Arbab, M. S.; Shah, J.;

Rehman, W. U. Green hydrogen storage and delivery: Utilizing highly active homogeneous and heterogeneous catalysts for formic acid dehydrogenation. *Int. J. Hydrogen Energy* **2022**, *47*, 11694−11724.

(20) (a) Agapova, A.; Alberico, E.; Kammer, A.; Junge, H.; Beller, M. Catalytic Dehydrogenation of Formic Acid with Ruthenium-PNP-Pincer Complexes: Comparing N-Methylated and NH-Ligands. *ChemCatChem* **2019**, *11*, 1910−1914. (b) Patra, S.; Singh, S. K. Hydrogen Production from Formic Acid and Formaldehyde over Ruthenium Catalysts in Water. *Inorg. Chem.* **2020**, *59*, 4234−4243. (c) Kar, S.; Rauch, M.; Leitus, G.; Ben-David, Y.; Milstein, D. Highly efficient additive-free dehydrogenation of neat formic acid. *Nat Catal.* **2021**, *4*, 193−201. (d) Patra, S.; Deka, H.; Singh, S. K. Bis-Imidazole Methane Ligated Ruthenium(II) Complexes: Synthesis, Characterization, and Catalytic Activity for Hydrogen Production from Formic Acid in Water. *Inorg. Chem.* **2021**, *60*, 14275−14285.

(21) (a) Fink, C.; Laurenczy, G. A Precious Catalyst: Rhodium-Catalyzed Formic Acid Dehydrogenation in Water. *Eur. J. Inorg. Chem.* **2019**, 2381−2387. (b) Hermosilla, P.; Urriolabeitia, A.; Iglesias, M.; Polo, V.; Casado, M. A. Efficient solventless dehydrogenation of formic acid by a CNC-based rhodium catalyst. *Inorg. Chem. Front*. **2022**, *9*, 4538−4547.

(22) (a) Wang, W.-H.; Wang, H.; Yang, Y.; Lai, X.; Li, Y.; Wang, J.; Himeda, Y.; Bao, M. Synergistic Effect of Pendant N Moieties for Proton Shuttling in the Dehydrogenation of Formic Acid Catalyzed by Biomimetic Ir^{III} Complexes. *ChemSusChem* **2020**, *13*, 5015−5022. (b) Liu, H.; Wang, W.-H.; Xiong, H.; Nijamudheen, A.; Ertem, M. Z.; Wang, M.; Duan, L. Efficient Iridium Catalysts for Formic Acid Dehydrogenation: Investigating the Electronic Effect on the Elementary β-Hydride Elimination and Hydrogen Formation Steps. *Inorg. Chem.* **2021**, *60*, 3410−3417. (c)

Luque-Gómez, A.; García-Abellán, S.; Munarriz, J.; Polo, V.; Passarelli, V.; Iglesias, M. Impact of Green Cosolvents on the Catalytic Dehydrogenation of Formic Acid: The Case of Iridium Catalysts Bearing NHC-phosphane Ligands. *Inorg. Chem.* **2021**, *60*, 15497−15508. (d) Mo, X.-F.; Liu, C.; Chen, Z. W.; Ma, F.; He, P.; Yi, X. Y. Metal-Ligand Cooperation in Cp*Ir-Pyridylpyrrole Complexes: Rational Design and Catalytic Activity in Formic Acid Dehydrogenation and CO_2 Hydrogenation under Ambient Conditions. *Inorg. Chem*. **2021**, *60*, 16584−16592. (e) Lentz, N.; Albrecht, M. A Low-Coordinate Iridium Complex with a Donor-Flexible *O,N*-Ligand for Highly Efficient Formic Acid Dehydrogenation. *ACS Catal.* **2022**, *12*, 12627−12631. (f) Guzmán, J; Urriolabeitia, A.; Polo, V.; Fernández-Buenestado, M.; Iglesias, M.; Fernández-Alvarez F. J. Dehydrogenation of formic acid using iridium-NSi species as catalyst precursors. *Dalton Trans* **2022**, *51*, 4386−4393. (g) Ge, S.; Gong, L.; Yi, P.; Mo, X.; Liu, C.; Yi, X. Y.; He, P. N-Site Regulation of Pyridyltriazole in Cp*Ir(N̂N)(H_2O) Complexes Achieving Catalytic FA Dehydrogenation. *Inorg. Chem.* **2023**, *62*, 18375−18383. (h) Fernández-Buenestado, M.; Somerville, R. J.; López-Serrano, J.; Campos, J. A genuine germylene PGeP pincer ligand for formic acid dehydrogenation with iridium. *Chem. Commun.* **2023**, *59*, 8826−8829. (i) Guo, J.; Li, M.; Yin, C.; Zhong, D.; Zhang, Y.; Li, X.; Wang, Y.; Yuan, J.; Xie, H.; Qi, T. Formic Acid Dehydrogenation through Ligand Design Strategy of Amidation in Half-Sandwich Ir Complexes. *Inorg. Chem.* **2023**, *62*, 18982−18989.

(23) (a) Lentz, N.; Streit, Y.; Knörr, P.; Albrecht, M. Sterically and Electronically Flexible Pyridylidene Amine Dinitrogen Ligands at Palladium: Hemilabile *cis*/*trans* Coordination and Application in Dehydrogenation Catalysis. *Chem. Eur. J.* **2022**, *28*, e202202672. (b) Osipova, E. S.; Sedlova, D. V.; Gutsul, E. I.; Nelyubina, Y. V.; Dorovatovskii, P. V.; Epstein, L. M.; Filippov,

O. A.; Shubina, E. S.; Belkova, N. V. Reactivity of Heterobimetallic Ion Pairs in Formic Acid Dehydrogenation. *Organometallics* **2023**, *42*, 2651−2660.

(24) Esteruelas, M. A.; García-Yebra, C.; Martín, J.; Oñate, E. Dehydrogenation of Formic Acid Promoted by a Trihydride-Hydroxo-Osmium(IV) Complex: Kinetics and Mechanism. *ACS Catal.* **2018**, *8*, 11314−11323.

(25) Buil, M. L.; Cabeza, J. A.; Esteruelas, M. A.; Izquierdo, S.; Laglera-Gándara, C. J.; Nicasio, A. I.; Oñate, E. Alternative Conceptual Approach to the Design of Bifunctional Catalysts: An Osmium Germylene System for the Dehydrogenation of Formic Acid. *Inorg. Chem.* **2021**, *60*, 16860−16870.

(26) Esteruelas, M. A.; Oliván, M.; Oñate, E. Sigma-bond activation reactions induced by unsaturated Os(IV)-hydride complexes. *Avd. Organomet. Chem.* **2020**, *74*, 53−104.

(27) (a) Chatterjee, B.; Chang, W.-C.; Jena, S.; Werlé, C. Implementation of Cooperative Designs in Polarized Transition Metal Systems-Significance for Bond Activation and Catalysis. *ACS Catal.* **2020**, *10*, 14024−14055. (b) Elsby, M. R.; Baker, R. T. Strategies and mechanisms of metal-ligand cooperativity in first-row transition metal complex catalysts. *Chem. Soc. Rev.* ***2020,*** 49, 8933−8987.

(28) Esteruelas, M. A.; López, A. M.; Oñate, E.; Raga, E. Metathesis between E−C(sp^n) and H−C(sp^3) σ-Bonds (E = Si, Ge; n = 2, 3) on an Osmium-Polyhydride. *Angew. Chem. Int. Ed*. **2022**, *61*, e202204081.

(29) (a) Kozuch, S.; Shaik, S. A Combined Kinetic−Quantum Mechanical Model for Assessment of Catalytic Cycles: Application to Cross-Coupling and Heck Reactions. *J. Am. Chem. Soc*. **2006**,

128, 3355−3365. (b) Kozuch, S.; Martin, J. M. L. “Turning Over” Definitions in Catalytic Cycles. *ACS Catal.* **2012**, *2*, 2787−2794.

(30) (a) Scholten, J. D.; Prechtl, M. H. G.; Dupont, J. Decomposition of Formic Acid Catalyzed by a Phosphine-Free Ruthenium Complex in a Task-Specific Ionic Liquid. *ChemCatChem* **2010**, *2*, 1265−1270. (b) Zell, T.; Butschke, B.; Ben-David, Y.; Milstein, D. Efficient Hydrogen Liberation from Formic Acid Catalyzed by a Well-Defined Iron Pincer Complex under Mild Conditions. *Chem. Eur. J.* **2013**, *19*, 8068−8072. (c) Wang, W.-H.; Xu, S.; Manaka, Y.; Suna, Y.; Kambayashi, H.; Muckerman, J. T.; Fujita, E.; Himeda, Y. Formic Acid Dehydrogenation with Bioinspired Iridium Complexes: A Kinetic Isotope Effect Study and Mechanistic Insight. *ChemSusChem* **2014**, *7*, 1976−1983. (d) Wang, W.-H.; Ertem, M. Z.; Xu, S.; Onishi, N.; Manaka, Y.; Suna, Y.; Kambayashi, H.; Muckerman, J. T.; Fujita, E.; Himeda, Y. Highly Robust Hydrogen Generation by Bioinspired Ir Complexes for Dehydrogenation of Formic Acid in Water: Experimental and Theoretical Mechanistic Investigations at Different pH. *ACS Catal.* **2015**, *5*, 5496−5504. (e) Ertem, M. Z.; Himeda, Y.; Fujita, E.; Muckerman, J. T. Interconversion of Formic Acid and Carbon Dioxide by Proton-Responsive, Half-Sandwich Cp*Ir^{III} Complexes: A Computational Mechanistic Investigation. *ACS Catal.* **2016**, *6*, 600−609. (f) Iguchi, M.; Zhong, H.; Himeda, Y.; Kawanami, H. Kinetic Studies on Formic Acid Dehydrogenation Catalyzed by an Iridium Complex towards Insights into the Catalytic Mechanism of High-Pressure Hydrogen Gas Production. *Chem. Eur. J.* **2017**, *23*, 17017−17021.

(31) (a) Howard, J. A. K.; Johnson, O.; Koetzle, T. F.; Spencer, J. L. Crystal and Molecular Structure of Bis(diisopropylphenylphosphine)hexahydridoosmium, [$OsH_6(PC_{12}H_{19})_2$]: Single-Crystal Neutron Diffraction Study at 20 K. *Inorg. Chem.* **1987**, *26*, 2930−2933. (b) Esteruelas, M. A.; Lledós, A.; Martín, M.; Maseras, F.; Osés, R.; Ruiz, N.; Tomàs, J. Synthesis and

Characterization of Mixed-Phosphine Osmium Polyhydrides: Hydrogen Delocalization in $[OsH_5P_3]^+$ Systems. *Organometallics* **2001**, *20*, 5297−5309. (c) Esteruelas, M. A.; Lledós, A.; Maseras, F.; Oliván, M.; Oñate, E.; Tajada, M. A.; Tomàs, J. Preparation and Characterization of Osmium-Stannyl Polyhydrides: d^4-d^2 Oxidative Addition of Neutral Molecules in a Late Transition Metal. *Organometallics* **2003**, *22*, 2087−2096. (d) Esteruelas, M. A.; Lledós, A.; Maresca, O.; Oliván, M.; Oñate, E.; Tajada, M. A. Preparation and Full Characterization of a Tetrahydride-bis(stannyl)-osmium(VI) Derivative. *Organometallics* **2004**, *23*, 1453−1456. (e) Eguillor, B.; Esteruelas, M. A.; Oliván, M.; Puerta, M. Abnormal and Normal N-Heterocyclic Carbene Osmium Polyhydride Complexes Obtained by Direct Metalation of Imidazolium Salts. *Organometallics* **2008**, *27*, 445−450. (f) Alós, J.; Bolaño, T.; Esteruelas, M. A.; Oliván, M.; Oñate, E.; Valencia, M. POP-Pincer Osmium-Polyhydrides: Head-to-Head (*Z*)-Dimerization of Terminal Alkynes. *Inorg. Chem.* **2013**, *52*, 6199−6213. (g) Buil, M. L.; Cardo, J. J. F.; Esteruelas, M. A.; Fernández, I.; Oñate, E. An Entry to Stable Mixed Phosphine-Osmium-NHC Polyhydrides. *Inorg. Chem.* **2016**, *55*, 5062−5070.

(32) Barrio, P.; Esteruelas, M. A.; Lledós, A.; Oñate, E.; Tomàs, J. Influence of the Cis Ligand on the H−H Separation and the Rotation Barrier of the Dihydrogen in Osmium-Elongated Dihydrogen Complexes Containing an Ortho-Metalated Ketone. *Organometallics* **2004**, *23*, 3008−3015.

(33) Belkova, N. V.; Epstein, L. M.; Filippov, O. A.; Shubina, E. S. Hydrogen and Dihydrogen Bonds in the Reactions of Metal Hydrides. *Chem. Rev*. **2016**, *116*, 8545−8587.

(34) An alternative adduct to **7t** with the second formic acid molecule interacting with the free oxygen atom of the coordinated formate ligand is 3.2 kcal mol^{-1} less stable than **7t**. Furthermore,

as expected, the activation barrier for the sliding of the metal fragment through the O–C–H path in this other species increases to 26.9 kcal mol^{-1}; a value higher than that corresponding to the rate-determining step, the release of hydrogen.

TOC Graphic.

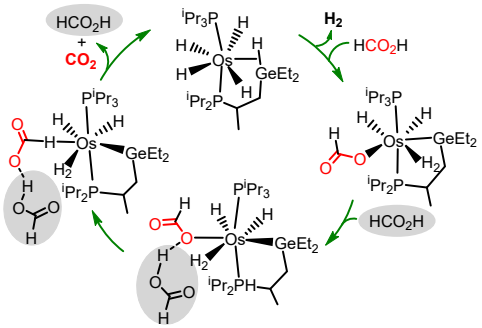
HCO2H
+
CO2
iPr3P
H
H
Os
H
GeEt2
iPr2P
H
H2
HCO2H
iPr3P
H
H
Os
GeEt2
H
O
O
H2
iPr2P
HCO2H
PiPr3
H
O
O
H
Os
H
GeEt2
H2
iPr2PH
PiPr3
H
H
Os
H
GeEt2
H2
iPr2P
O
O
H
O
O
H